ELSEVIER

Journal of Fluids and Structures 23 (2007) 767–785

JOURNAL OF FLUIDS AND STRUCTURES

www.elsevier.com/locate/jfs

Mechanics of a thin, tensioned shell, wrapped helically around a turn-bar

S. Müftü

Department of Mechanical and Industrial Engineering, Northeastern University, Boston, MA 02115, USA

Received 19 December 2005; accepted 25 November 2006
Available online 9 February 2007

Abstract

The fluid–structure interactions between a flexible web and an externally pressurized air cushion are modeled allowing for the possibility of contact. The web is wrapped around a porous, cylindrical turn-bar at an oblique angle (helically). The turn-bar supplies pressurized air into the web/turn-bar clearance to float the web. The shell model, developed to represent the mechanics of the web, allows it to be wrapped around the cylinder in a helical fashion. The fluid mechanics of the air in the web/turn-bar clearance is a two-dimensional form of the incompressible Navier–Stokes equations averaged in the clearance direction and augmented by nonlinear source terms. Contact between the web and the reverser, which is undesirable in a turn-bar application, is included in the model in order to enable the analysis of the limiting cases. The coupled equilibrium between fluid mechanics, shell deflections and contact is found numerically. This paper describes the theory. Case studies are conducted in order to understand the mechanics of the coupled system, and to make design recommendations. It is shown that the helix angle has a strong influence on the equilibrium configurations: increasing helix-angle results in increased web-reverser separation, while the air pressure settles to a lower value. This behavior is due to the reduced shell stiffness and belt-wrap pressure for the helically wrapped webs. Conditions that render a nearly uniform web/turn-bar clearance in the circumferential direction are identified. The supply pressure and airflow rates necessary to prevent web-scratches are calculated.

Keywords: Helically wrapped shell; Web mechanics; Turn-bar; Air reverser

1. Introduction

Thin, flexible, continuous structures such as paper, various forms of films, metal sheets and magnetic tapes are generally known as webs. These materials are typically processed at high transport speeds (1–20 m/s), under tension (10–200 N/m). An *air-reverser* is used in a web handling application along the path of the web, where its transport direction needs to be reversed without making contact with a rigid surface (Fig. 1(a)). In order to achieve this goal, the web is wrapped around a cylindrical drum with holes on its surface to provide a pressurized air layer under the web. The equations governing the fluid mechanics in the web/air-reverser clearance were given by Müftü et al. (1998), and Müftü and Cole (1999) introduced a model to analyze fluid–structure interactions between the web and the airflow from an air-reverser.

E-mail address: s.muftu@neu.edu.

0889-9746/$ - see front matter © 2007 Elsevier Ltd. All rights reserved.
doi:10.1016/j.jfluidstructs.2006.11.007

Nomenclature

$a_{\alpha\beta}$	metric tensor
$\vec{a}_\alpha$	tangent vectors in curvilinear coord. ($\alpha = 1, 2$)
$b_{\alpha\beta}$	curvature tensor
c	web thickness, m
$\vec{e}_i$	Cartesian base vectors ($i = 1, 2, 3$)
D_b, D_t, D_s	bending rigidity, in-plane and shear stiffness of the web
E	elastic modulus of the web, Pa
$E_{\alpha\beta}$	total in-plane strain ($\alpha, \beta = x, y$)
$e_{\alpha\beta}$	membrane strain ($\alpha, \beta = x, y$)
F_x, F_y, F_z	external tractions acting on the web, Pa
H	web/air-reverser clearance, m
L_1, L_2	web tangency points at $y = 0$, m
L_x, L_y	length and width of the web, m
L'_x, L'_y	length and width of the fluid domain, m
$M_{\alpha\beta}$	bending moment ($\alpha, \beta = x, y$)
$N_{\alpha\beta}$	in-plane stress resultant ($\alpha, \beta = x, y$)
$N'_{\alpha\beta}$	in-plane stress resultant ($\alpha, \beta = x, y$)
n, $\vec{n}$	normal curvilinear coordinate and base vector
p_0	supply pressure, Pa
p, p_c	air pressure, contact pressure, Pa
P_a	contact compliance, Pa
p_{net}	air pressure acting on the web, Pa
Q_α	shear force resultant ($\alpha = x, y$)
$R(x,y)$	web radius, m
R_c	radius of the air-reverser, m
S	middle surface of the web
T	longitudinal external tension, N/m
U	air discharge velocity at the holes, m/s
U_0	$(p_0/2\rho)^{1/2}$ reference discharge velocity, m/s
u', v'	air velocities in x' and y' directions, m/s
u_1, u_2	in-plane curvilinear coordinates
v_1, v_2	in-plane web deflections
$\bar{w} = w - w_r$	web disp. with respect to reference state, m
w	web disp. with respect to initial state, m
w_r	$w(x,L_y/2)$ reference web displacement, m
x, y	coordinate system for the web equations
x', y'	coordinate system for the air equations
$\alpha(x', y')$	areal hole density
β	helical wrap angle, deg.
γ	shear strain
δ	initial web-reverser clearance, m
θ_w	wrap angle of the web
θ_{F1}, θ_{F2}, θ_{F3}, θ_{F4}	limits of the hole-region in circ-dir. on the reverser, deg.
κ	discharge loss coefficient
$\kappa_{\alpha\beta}$	web curvature ($\alpha = x, y$)
ν	Poisson's ratio of the web
ρ	air density, kg/m^3
σ_a	contact engagement (asperity) height (m)
τ'_{xy}, τ'_{zy}, τ'_{zy}	fluid shear stress, Pa
τ'_x, τ'_y	fluid normal stresses, Pa

The web is wrapped around an air-reverser in such a way that its transport (longitudinal) direction is perpendicular to the axis of the air reverser. In another type of non-contact web support device, known as a *turn-bar*, the web is wrapped around the cylinder in a helical fashion with a helix-angle β (Fig. 1(b)). This device allows the web transport direction to be changed by an angle 2β, and thus enables more flexibility on manufacturing floor layout. In both applications the web is transported in its longitudinal direction under an externally applied tension T. In this paper, a more general model for the web mechanics is introduced, where the web approaches the reverser at an oblique angle, as shown in Fig. 1(b).

The fluid–structure interaction between the flexible web and surrounding air is typically unavoidable and gives rise to interesting problems. A flexible web drags the surrounding air into the guide-web interface while it travels over rollers

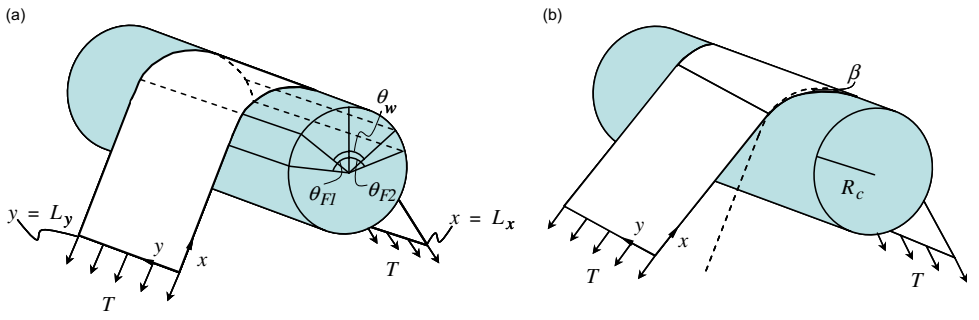

Fig. 1. Schematic representation of a web wrapped around (a) an air-reverser, and (b) a turn-bar, under tension T.

or stationary guides. The resulting phenomenon is known as the *foil bearing* problem and has been extensively studied (Ducotey and Good, 1999; Müftü and Altan, 2000; Hashimoto and Nakagawa, 2001). The foil bearing problem stems from low Reynolds number effects, hence the fluid mechanics is governed by the Reynolds lubrication equation (Gross, 1980).

In both air-reverser and turn-bar applications, pressurized air is introduced between the flexible web and the rigid cylinder from the holes on the surface of the cylinder. The clearance between the web and the cylinder is typically on the order of 3 mm. The flow is inertia-dominated with the possibility of turbulent regions near the outer periphery of the clearance (Müftü and Cole, 1999). The air pressure and the web deflections are coupled. The air pressure is primarily balanced with respect to the belt-wrap pressure (T/R_c) acting on the web due to the external tension, where R_c is the radius of the air-reverser. However, creating a flow pattern under the web, which will balance the belt-wrap pressure, is a challenging task. The air pressure and flow pattern primarily depend on the distribution pattern of the holes on the surface of the reverser. While the flow could stagnate in the central wrap-region and provide an air cushion with a fairly uniform pressure, along the four edges of the wrap-region air could flow from underneath the web with speeds reaching 25–30 m/s. A two-dimensional (2-D) air-flow model, in the plane of the web, has been introduced by Lewis and reported by Müftü et al. (1998).

In order to derive the equilibrium equations for a web in an air-reverser application, Müftü and Cole (1999) took into account the following steps the web takes until it finds equilibrium with a steady-state clearance. A detailed description of their model is given in their paper, and described here for completeness. The web, which is initially flat, is first wrapped around the cylinder, under tension T. This configuration forms the *initial reference state*, w_0. At this state, the effect of airflow is neglected. Once the air starts coming into the interface through the holes located on the cylinder (air-reverser) surface, the web deflects away from the initial reference state. During this deflection, the web tension is kept constant by a control mechanism, which allows the web length to increase between the two support-rollers on the entry and exit sides of the reverser. The web eventually finds a steady-state condition which is removed from the reverser surface on the order of few millimeters. Thus, the final reference state of the web from which the web deflections are measured is removed from the initial reference state and depends on the conditions such as tension and air pressure distribution of the particular application. This reference state, which is initially unknown, is called the *self-adjusting reference state*, w_r. The web deflections are measured with respect to the self-adjusting reference state. As this state is not known *a priori*, the web deflection equations become nonlinear. The self-adjusting reference state is a cylindrical surface extending from the mid-line of the deflected web defined as $w_r(x) = w(x,L_x/2)$. The normal component of the web deflection is measured with respect to w_r and is indicated by $\bar{w} = w - w_r$.

In this paper, the equation governing the mechanics of a flexible shell, wrapped helically around a cylinder with flat parts at the leading and trailing sides is derived. This derivation follows Rongen (1994) and Müftü and Cole (1999). The equations governing the fluid flow in the web/turn-bar clearance, reported below, are essentially the same equations given by Müftü and Cole (1999), with modified boundaries as described. The coupled fluid and web equations are solved numerically as described by Müftü (1999).

2. Theory

2.1. Coordinate systems used in the model

The geometry of a web wrapped at an oblique (helix) angle β around a cylinder of radius R_c is depicted in Fig. 1. Note that the web and the air-reverser surface can be rolled out on a plane as shown in Fig. 2(a). The extent of the circumferential wrap is given by the *wrap-angle* θ_w as shown in this figure. The *wrap-region* spans the length $R_c\theta_w$. The projection of the *hole-region* from the air-reverser onto the web is indicated by the span $R_c(\theta_{F1}+\theta_{F4})$. The web deformation is calculated in the solution domain Ω_w, defined as

$$\{(x,y) \in \Omega_w \subset R^2 | 0 \leqslant x \leqslant L_x,\ 0 \leqslant y \leqslant L_y\}. \tag{1}$$

The length (L_x) and the width (L_y) of this domain are defined in Fig. 2(b). The fluid mechanics equations are expressed in solution domain Ω_f on the cylindrical reverser, not shown here. The interpolation of the variables h and p between the two solution meshes is performed on the (x', y') coordinate system shown in Fig. 2(b). The projection of Ω_f on Ω_w is $\Omega_{f\to w}$ and it is defined as

$$\{(x,y) \in \Omega_{f\to w} \subset \Omega_w | y \tan\beta + x - L_{F1} \geqslant 0 \wedge y \tan\beta + x - L_{F2} \leqslant 0\}, \tag{2}$$

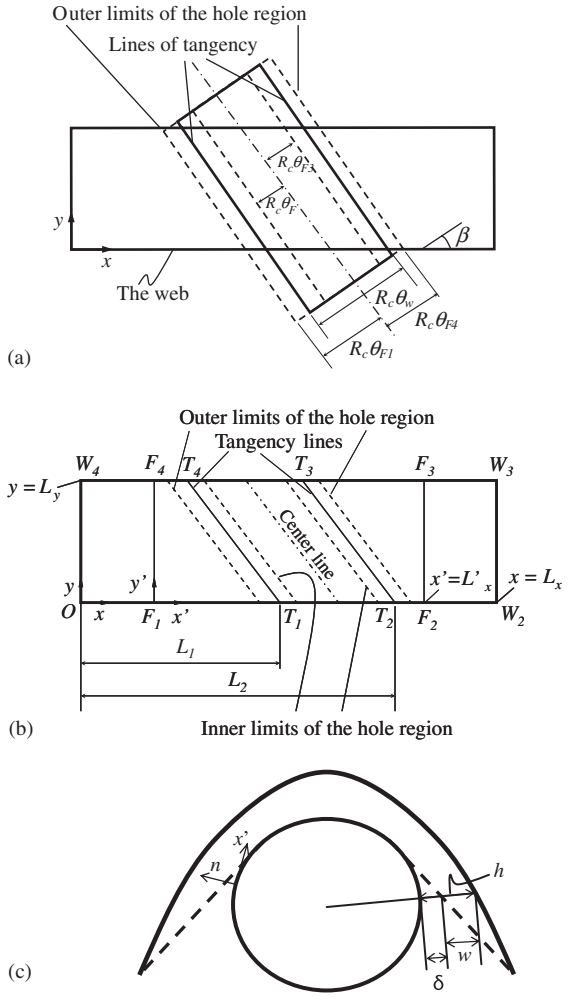

Fig. 2. (a) A schematic depiction of the web and the reverser rolled-out on a plane. (b) The geometric definitions used to define the web Ω_w and fluid Ω_f domains. (c) The web/turn-bar clearance h.

where

$$L_{F1} = L_1 - R\left\{\frac{\tan(\theta_{F1} - \frac{1}{2}\theta_w)}{\cos\beta}\right\} \quad \text{and} \quad L_{F2} = L_2 + R\left\{\frac{\tan(\theta_{F4} - \frac{1}{2}\theta_w)}{\cos\beta}\right\}.$$

The lengths L_{F1} and L_{F2} are the projections of the outer limits of the hole-regions on the web.

The geometry can be described, as shown in Fig. 2(b), as the union of two flat sections ($OT_1T_4W_4$ and $T_2W_2W_3T_3$) on the entry and exit sides of the wrap-region, with the wrap-region ($T_1T_2T_3T_4$). This figure shows the projections of the tangency points and the limits of the hole-region on the unwrapped configuration of the web, where the lines T_1T_4 and T_2T_3 are the lines of tangency.

2.2. Equations of equilibrium for a helically wrapped web

A web wrapped around a cylindrical surface with a helix-angle β represents a developable surface. Web equilibrium equations are derived in curvilinear coordinates, described by Rongen (1994). The curvilinear coordinates are assumed to coincide with the initial reference configuration w_0, for an infinitely thin web. The equations of equilibrium are derived using the Kirchhoff–Love assumptions (Timoshenko and Woinkowsky-Krieger, 1987).

2.2.1. Geometry of a helical shell

The geometry of a shell is described by its middle-surface S and thickness c. In a 3-D space, with Cartesian basis vectors $\{\vec{e}_1, \vec{e}_2, \vec{e}_3\}$ and origin O, a generic middle surface, is described by two independent surface coordinates u_1, and u_2 as follows:

$$\vec{r} = \vec{r}(u_1, u_2) = r_i(u_\alpha)\vec{e}_i, \tag{3}$$

where the Latin indices take the values 1, 2, 3 and the Greek indices take the values 1 and 2. The summation convention applies to this equation where the repeated indices are summed. The location of any point $\vec{x}$ in the curved shell can then be defined by its *normal coordinates* (u_1, u_2, u_3),

$$\vec{x}(u_1, u_2, u_3) = \vec{r}(u_1, u_2) + u_3\vec{n}(u_1, u_2), \tag{4}$$

where $\vec{r}(u_1, u_2)$ is the position vector to a point on the middle surface, $\vec{n}$ is the unit normal on the middle surface at this point, and $-c/2 \leqslant u_3 \leqslant c/2$. The middle-surface S is located at $u_3 = 0$. The *tangent vectors* to this middle surface are defined by

$$\vec{a}_\alpha = \vec{r}_{,\alpha} = \frac{\partial \vec{r}}{\partial u_\alpha}, \tag{5}$$

which form the base vectors for the 2-D tangent plane, at each point. The *normal vector* to the middle surface is given by

$$\vec{n} = \frac{\vec{a}_1 \times \vec{a}_2}{|\vec{a}_1 \times \vec{a}_2|}, \tag{6}$$

providing $\vec{n} \cdot \vec{a}_\alpha = 0$ at every point of the surface. The first fundamental tensor or metric tensor of the surface is defined by

$$a_{\alpha\beta} = \vec{a}_\alpha \cdot \vec{a}_\beta. \tag{7}$$

The second fundamental tensor or the curvature tensor of the surface is

$$b_{\alpha\beta} = \vec{a}_{\alpha,\beta} \cdot \vec{n}. \tag{8}$$

In order to calculate the value of $\vec{a}_\alpha$ and $\vec{n}$ for the helical geometry, let us investigate the equation of the line wrapped around a cylinder with the helix-angle β as shown in Fig. 3. Let the curvilinear coordinates (u_1, u_2) be oriented along and perpendicular to this line, respectively. The point P on the cylindrical surface can be represented in terms of u_1, and u_2, and Eq. (3) as follows:

$$\vec{r} = R\cos\varphi\vec{e}_1 + R\sin\varphi\vec{e}_2 + (u_1\sin\beta + u_2\cos\beta)\vec{e}_3, \tag{9}$$

with

$$\varphi = (u_1\cos\beta - u_2\sin\beta)/R.$$

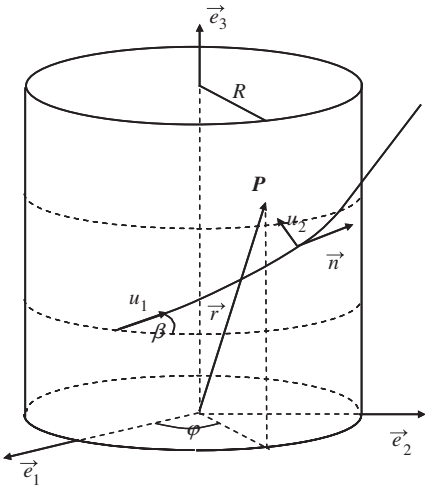

Fig. 3. Coordinates of a point P on Cartesian, $\vec{e}_1, \vec{e}_2, \vec{e}_3$, and curvilinear, $\vec{u}_1, \vec{u}_2, \vec{n}$, coordinate systems.

The tangent and normal vectors for this surface are found from Eqs. (5), (6) and (9) as follows:

$$\vec{a}_1 = -\sin\varphi\cos\beta\vec{e}_1 + \cos\varphi\cos\beta\vec{e}_2 + \sin\beta\vec{e}_3, \quad \vec{a}_2 = \sin\varphi\sin\beta\vec{e}_1 - \cos\varphi\sin\beta\vec{e}_2 + \cos\beta\vec{e}_3,$$
$$\vec{n} = \cos\varphi\vec{e}_1 + \sin\varphi\vec{e}_2. \tag{10}$$

The metric and the curvature tensors become

$$a_{\alpha\beta} = \begin{bmatrix} 1 & 0 \\ 0 & 1 \end{bmatrix}, \quad b_{\alpha\beta} = \frac{1}{R}\begin{bmatrix} -\cos^2\beta & \sin\beta\cos\beta \\ \sin\beta\cos\beta & -\sin^2\beta \end{bmatrix}. \tag{11}$$

These relations are used next to develop the equations governing the web static equilibrium equations for the helically wrapped web under tension T. Shell theory is based on the Kirchhoff–Love assumptions which state that (a) the shell is in a state of plane stress, where the normal stress in the thickness direction of the shell is neglected; and (b) a fiber of the shell which is initially straight and normal to the middle-surface S, remains straight and normal to the middle surface after deformation (Timoshenko and Woinkowsky-Krieger, 1987).

The in-plane displacements of the shell are indicated by v_α, and the out-of-plane displacement is by w. The strain–displacement relations for the shell then become

$$E_{\alpha\beta} = e_{\alpha\beta} - u_3\kappa_{\alpha\beta}, \quad E_{\alpha 3} = \gamma_\alpha,$$
$$e_{\alpha\beta} = v_{\alpha,\beta} - b_{\alpha\beta}\bar{w} + \frac{1}{2}\bar{w}_\alpha\bar{w}_\beta, \quad \kappa_{\alpha\beta} = \bar{w}_{\alpha\beta} + b_{\alpha\beta}, \quad \gamma_\alpha = \bar{w}_\alpha, \tag{12}$$

where $E_{\alpha\beta}$ is the total-strain, $e_{\alpha\beta}$ is the membrane-strain, γ_α is the shear-strain, $\kappa_{\alpha\beta}$ is the curvature of the middle surface. Note that the curvature $b_{\alpha\beta}$ is added to the curvature of the middle surface in order to take into account the initial bending of the web around the cylindrical surface.

The in-plane stresses in the deformed shell are indicated by $\sigma_{\alpha\beta}$ and the shear stresses in the direction normal to the middle-surface S are indicated by $\sigma_{\alpha\beta}$. The shell theory is based on stress resultants which are defined as

$$(N_{\alpha\beta}, M_{\alpha\beta}, Q_\alpha) = \int_{-c/2}^{c/2} (\sigma_{\alpha\beta}, u_3\sigma_{\alpha\beta}, \sigma_{\alpha 3})\,\mathrm{d}u_3, \tag{13}$$

where $N_{\alpha\beta}$ are the in-plane stress resultants, $M_{\alpha\beta}$ are the bending moment resultants and Q_α are the normal shear stress resultants. The static equilibrium of a curved shell is given by the following set of equations:

$$N_{\alpha\beta,\beta} + F_\alpha = 0, \tag{14a}$$

$$Q_{\alpha,\beta} + (w_\alpha N_{\alpha\beta}) + b_{\alpha\beta}N_{\alpha\beta} + F_z = 0, \tag{14b}$$

$$M_{\alpha\beta,\beta} - Q_\alpha + C_\alpha = 0, \tag{14c}$$

where F_α, C_α and F_z are the externally applied in-plane tractions, bending moment and pressure, respectively. Eqs. (14a,b) represent the static equilibrium of in-plane and out-of-plane forces, respectively. Eq. (14c) represents the moment equilibrium at steady state.

For an isotropic shell the constitutive equations are:

$$N_{\alpha\beta} = D_t[(1-\nu)e_{\alpha\beta} + \nu a_{\alpha\beta}e_{\gamma\gamma}], \tag{15a}$$

$$M_{\alpha\beta} = -D_b[(1-\nu)\kappa_{\alpha\beta} + \nu a_{\alpha\beta}\kappa_{\gamma\gamma}], \tag{15b}$$

$$Q_\alpha = D_s\gamma_\alpha, \tag{15c}$$

where $D_b = Ec^3/12(1-\nu^2)$ is the bending rigidity, $D_t = Ec/(1-\nu^2)$ the in-plane stiffness and $D_s = \kappa Gc$ the shear stiffness, with the Young's modulus E, shear modulus G and shear correction coefficient κ. The correction coefficient usually takes the value of 5/6.

The mechanics of the web is described with respect to a set of curvilinear coordinates located on the web (x, y, n) (Fig. 2). In order to describe the curved part of the web, a set of coordinate axes (u_1, u_2, n) are fixed on the helically wrapped part of the web (Fig. 3). This allows the derivation of the web mechanics in the helically wrapped region. As the (x, y, n) axis directions are coincident with the (u_1, u_2, n), the upcoming derivation is simplified; the only difference between the flat and curved sections of the web will be based on the presence or lack thereof of the curvature $1/R_c$. After combining Eqs. (14b) and (14c), the equilibrium equations become

$$N_{\alpha\beta,\beta} + F_\alpha = 0, \quad M_{\alpha\beta,\alpha\beta} + (w_\alpha N_{\alpha\beta})_\beta + b_{\alpha\beta}N_{\alpha\beta} + F_z = 0. \tag{16}$$

By using moment curvature relations, (15b), and the curvature tensor (11), Eq. (16) becomes:

$$N_{xx,x}+N_{xy,y}+F_x=0,\quad N_{yx,x}+N_{yy,y}+F_y=0,$$
$$D_b\nabla^4\bar{w}-\left(w_{xx}-\frac{\cos^2\beta}{R_w}\right)N_{xx}-2\left(w_{xy}-\frac{\sin\beta\cos\beta}{R_w}\right)N_{xy}-\left(w_{yy}-\frac{\sin^2\beta}{R_w}\right)N_{yy}=F_z, \tag{17}$$

where $R_w=R_w(x,y)$ is the curvature of the shell defined as

$$\frac{1}{R_w(x,y)}=\begin{cases}0, & \text{for } x+y\tan\beta-L_1<0,\\ \dfrac{1}{R_c}, & \text{for } x+y\tan\beta-L_1\geqslant 0 \quad\text{and}\quad x+y\tan\beta-L_2\leqslant 0,\\ 0, & \text{for } x+y\tan\beta-L_2>0,\end{cases} \tag{18}$$

in which L_1 and L_2 are the tangency points at $y=0$ (Fig. 2(b)). Eqs. (17) represent a set of coupled partial differential equations, which in turn represent the equilibrium of a shell wrapped around a cylinder in a helical fashion, with a helix-angle β, as described in Fig. 1, subjected to in-plane tractions F_x and F_y and external pressure p. Note that in obtaining this equation the nonlinear terms $\bar{w}(\partial^2 w/\partial x^2)$, $(\partial\bar{w}/\partial x)^2$, $(\partial\bar{w}/\partial y)^2$ have been neglected in order to linearize the governing equation. This should not affect the results as long as the deflections are on the order of the web thickness; however, these terms should be kept in the analysis to retain the ability to model large deflections in the future. Moreover, the in-plane external tractions, F_x and F_y, are assumed to be zero.

In a typical web handling application, the web is pre-tensioned to a value T in the longitudinal direction. It is assumed that, in the undeformed state, only T exists as in-plane stress, when the web is wrapped around the cylinder. The in-plane stress resultants after deformation are indicated as follows:

$$N_{xx}=T+N'_{xx},\quad N_{yy}=N'_{yy},\quad N_{xy}=N'_{xy}. \tag{19}$$

A simplified equation which represents the equilibrium of out-of-plane force resultants and bending moments can be obtained by considering that N'_{xx} can be evaluated in terms of deformations by using the strain-displacement relations (12) and the constitutive relation (15). Thus, the in-plane stress resultant in the longitudinal direction becomes

$$N_{xx}=T+D_t\left[\frac{\bar{w}}{R_w}\cos^2\beta+\frac{1}{2}\bar{w}_{,x}^2+\upsilon\left(\frac{\bar{w}}{R_w}\sin^2\beta+\frac{1}{2}\bar{w}_{,y}^2\right)\right]. \tag{20}$$

Then, using the above equations it can be shown that the equation of equilibrium for a flexible web wrapped around a cylindrical drum with a helix-angle β, becomes

$$D_b\nabla^4\bar{w}+D_t(\cos^4\beta+\upsilon\cos^2\beta\sin^2\beta)\frac{\bar{w}}{R_w^2(x,y)}-Tw_{xx}=p+p_c-\frac{T\cos^2\beta}{R_w}. \tag{21}$$

For $\beta=0$, this equation reduces to the same web equilibrium equation derived for the case of no helix angle (Müftü and Cole, 1999). Note that the effect of the in-plane stress resultants N_{yy} and N_{xy} are neglected as they are small as compared to the longitudinal tension. In Eq. (17), the vertical component of the external traction F_z is replaced with the air pressure p and the contact pressure p_c. The air and contact pressure distributions are obtained from the solution of the fluid mechanics equations, and evaluation of the contact conditions as presented in the next sections.

The web is supported by a roller on each of its two longitudinal ends, and is free on its lateral edges. These conditions are represented as simple support conditions:

$$\bar{w}=0,\quad M_x=D_b(\bar{w}_{,xx}+\upsilon\bar{w}_{,yy})=0, \tag{22}$$

at $0\leqslant y\leqslant L_y$ and $x=0$, L_x, and as free boundary conditions:

$$M_y=D_b(\bar{w}_{,yy}+\upsilon\bar{w}_{,xx})=0,\quad Q_y=D_b(\bar{w}_{,yyy}+(2-\upsilon)\bar{w}_{,xxy})=0, \tag{23}$$

at $y=0$, L_y and $0\leqslant x\leqslant L_x$.

2.2.2. Initial clearance

The clearance $h(x,y)$ between the web and the turn-bar depends on the initial clearance $\delta(x,y)$ and the web displacement w (Fig. 2(c)):

$$h(x,y)=w(x,y)+\delta(x,y). \tag{24}$$

The initial clearance in the downstream and upstream sides of the web is obtained by calculating the distance between the web and the cylinder. In the wrap-region, the initial clearance is zero. This is expressed by the following relation:

$$\delta(x,y)=\begin{cases}[(x+y\tan\beta-L_1)^2\cos^2\beta+R_c^2]^{1/2}-R_c, & \{(x,y)\in\Omega_w | y\tan\beta+x-L_1<0\},\\ 0, & \{(x,y)\in\Omega_w | y\tan\beta+x-L_1\geqslant 0\wedge y\tan\beta+x-L_2\leqslant 0\},\\ [(x+y\tan\beta-L_2)^2\cos^2\beta+R_c^2]^{1/2}-R_c, & \{(x,y)\in\Omega_w | y\tan\beta+x-L_2>0\}.\end{cases} \tag{25}$$

In obtaining the equations for the curvature and the initial clearance, the effect of bending rigidity of the web is neglected; and, the web is assumed to consist of two flat segments and one "helically wrapped cylindrical" segment.

2.3. Equations of fluid mechanics

The steady-state form of the equations governing the fluid mechanics in the clearance between the web and the turn-bar were derived by Lewis (Müftü et al., 1998). As the clearance $h(x',y')$ between the web and the reverser is considerably smaller as compared to the other two dimensions of the fluid domain, namely x' and y' directions, the flow is assumed 2-D in the plane of the reverser. Thus, the flow velocities u' and v' in the x' and y' directions, respectively, are averaged in the direction of the clearance height, and the flow component in the z' direction is neglected. The effect of the air coming into the interface through the holes is modeled as a distributed source, indicated by $\alpha(x',y')$. Velocity U of air coming through each hole is a function of the supply pressure inside the reverser p_0 and the local pressure of air p. The 2-D flow assumption is invalid near each hole, and losses due to discharge are represented with the discharge coefficient κ, whose value lies in the range $0<\kappa<1$. The air velocity through each hole is modeled as

$$U=\kappa U_0\left(1-\frac{p}{p_0}\right)^{1/2}, \tag{26}$$

where the reference discharge velocity is $U_0=(p_0/2\rho)^{1/2}$. The conservation of mass in the web/turn-bar clearance is given by

$$\frac{\partial hu'}{\partial x'}+\frac{\partial hv'}{\partial y'}=\alpha U, \tag{27}$$

where the term on the right-hand side represents the mass of air coming into the interface through the air holes. The conservation of momentum in the x' and y'directions is represented by the following two equations:

$$\begin{aligned}&\rho\left(u'\frac{\partial u'}{\partial x'}+v'\frac{\partial u'}{\partial y'}\right)+\frac{\partial p}{\partial x'}-\mu\left(\frac{4}{3}\frac{\partial^2 u'}{\partial x'^2}+\frac{\partial^2 u'}{\partial y'^2}+\frac{1}{3}\frac{\partial^2 v'}{\partial x'\partial y'}\right)+2\frac{\tau_{z'x'}}{h}+\alpha\rho U\frac{u'}{h}=0,\\ &\rho\left(u'\frac{\partial v'}{\partial x'}+v'\frac{\partial v'}{\partial y'}\right)+\frac{\partial p}{\partial y'}-\mu\left(\frac{\partial^2 v'}{\partial x'^2}+\frac{4}{3}\frac{\partial^2 v'}{\partial y'^2}+\frac{1}{3}\frac{\partial^2 u'}{\partial x'\partial y'}\right)+2\frac{\tau_{z'y'}}{h}+\alpha\rho U\frac{v'}{h}=0,\end{aligned} \tag{28}$$

where ρ is the mass density, μ the viscosity of air, and p the air pressure averaged over the normal direction.

Gross (1980) discusses the dimensional analysis of the complete 3-D Navier–Stokes and mass conservation equations leading to *Reynolds' lubrication equation*, and shows that for this type of flow the proper nondimensional parameter representing the ratio of the inertial forces to viscous forces in the flow is the *modified Reynolds number*, $\mathrm{Re}^*=\rho Vh^2/\mu L$. The modified Reynolds number can be obtained from the Reynolds number for more general flow, $\mathrm{Re}=\rho Vh/\mu$ as $\mathrm{Re}^*=\mathrm{Re}(h/L)$. This in fact is an indication of the effect of the clearance-to-length ratio (h/L) on the lubricating flow.

Having said this, for the case discussed here, the following values are found: $\mathrm{Re}^*=20$, $\mathrm{Re}=5000$ for $\rho=1.2\,\mathrm{kg/m^3}$, $h=4\,\mathrm{mm}$, $L=1\,\mathrm{m}$, $\mu=1.85\times10^{-5}\,\mathrm{Pa\,s}$ and $V=20\,\mathrm{m/s}$. Thus, it is concluded that the flow is inertia dominated, and that the flow could be turbulent in the regions where the flow velocity attains its highest values, such as the outer periphery of the flow region.

In this model, the shear stresses $\tau_{z'x'}$ and $\tau_{z'y'}$ are found from the 1/7th-power–velocity distribution law for turbulent flow in a 2-D channel (Schilchting, 1987):

$$\tau_{z'x'}=\frac{1}{2}\rho 0.0676\cos\bar{\theta}\left(\frac{\rho h}{\mu}\right)^{\lambda'}(u'^2+v'^2)^{(2-\lambda')/2},\quad \tau_{z'y'}=\frac{1}{2}\rho 0.0676\cos\bar{\theta}\left(\frac{\rho h}{\mu}\right)^{\lambda'}(u'^2+v'^2)^{(2-\lambda')/2}, \tag{29}$$

with $\bar{\theta}=\tan^{-1}(u'/v')$ and $\lambda'=\frac{1}{4}$. However, a more complete model would consider turbulence models such as the k–ε model. The solution of this equation is discussed in Müftü et al. (1997).

The boundary Γ_f of the fluid solution domain is the outer periphery of the parallelogram, shown in Fig. 2(b), defined as

$$\left\{\Gamma_f|(x',y')\in\Omega_f\subset R^2,\quad (x',0)\wedge(x',L'_y)\wedge y'\tan\beta+x'-L'_{F1}=0\wedge y'\tan\beta+x'-L'_{F2}=0\right\}, \tag{30}$$

where $L_{F1}{}^*$ and $L_{F2}{}^*$ are the limits of the hole-regions at $y^*=0$. Given these, the boundary condition for the fluid becomes

$$p+\frac{1}{2}\kappa_B[(u')^2+(v')^2]=0\quad \text{on } \Gamma_f, \tag{31}$$

where κ_B is the boundary discharge coefficient.

2.4. Contact pressure

In case rigid body contact occurs between the web and the reverser surface, the web is supported (partially) by the contact pressure p_c. Whether contact will take place depends on the overall equilibrium of the web and the air pressure. If contact occurs, its magnitude, and location are not known *a priori*. In general, surfaces are not smooth; and contact between two surfaces takes place on the peaks of the surface asperities. A review of available multi-asperity contact models is beyond the scope of this paper. However, in the context of web and tape mechanics, papers by Rice et al. (2002), Lacey and Talke (1992) and Wu and Talke (1996) could be consulted for more information. In this work, the parabolic contact model introduced by Lacey and Talke for tape mechanics is used. This model was later evaluated by Rice et al. (2002) for contact of paper- and PET-based webs. In this model, the contact pressure is calculated by

$$p_c=P_a\left(1-\frac{h}{\sigma_a}\right)^2\quad \text{if } h\leqslant\sigma_a, \tag{32}$$

where P_a is the asperity compliance and σ_a the asperity engagement height. It is assumed that asperity contact takes place when the web-to-reverser clearance h falls below σ_a. The values of P_a and σ_a are typically empirically determined. Rice et al. (2002) provide these values for contact of various types of webs with a typical metal guide surface. In this paper, the following values were used: $P_a=1\times10^6\,\text{Pa}$ and $\sigma_a=100\times10^{-6}\,\text{m}$.

2.5. Coupled solution

The steady-state equilibrium between a nontranslating web and the air flow in the web turn-bar interface is modeled. The fluid-to-web coupling requires that the velocities and the tractions at the coupling interface, $n=h$ as described in Fig. 2(c), be continuous. In general, the velocity continuity requirement is expressed as follows:

$$u'=\frac{\partial v_1}{\partial t},\quad v'=\frac{\partial v_2}{\partial t}\quad\text{and}\quad w'=\frac{\partial w}{\partial t}\quad\text{at } n=h, \tag{33}$$

and the traction continuity requirement is expressed as follows:

$$\tau'_{zx}=F_x,\quad \tau'_{zy}=F_y\quad\text{and}\quad p=F_z\quad\text{at } n=h. \tag{34}$$

The effect of the fluid shear tractions on the in-plane web equilibrium, at the steady state, is typically considered to be negligible; and, therefore, as mentioned before, F_x and F_y are neglected. Due to the steady-state assumption, the time-derivatives of the web displacements are zero. This implies that on the web surface, $n=h$, the flow velocity should be $u'=v'=0$. The simplified fluid model used here assumes that u' and v' are constant through the clearance direction, and thus does not exactly comply with the velocity boundary condition. This discrepancy should be corrected in the future. In summary, the present model assumes that the web and the fluid are only coupled through the air pressure p directly and the clearance height h indirectly.

The coupled fluid–structure interactions which include the possibility of contact are found by solving Eqs. (17), (22)–(24), (27), (28) and (32) simultaneously. The solution method involves finite-difference discretization of the web-domain, and a pseudo-transient solution of the fluid-domain (Müftü and Cole, 1999). The nonlinear contact is handled by a standard Newton–Raphson algorithm (Müftü and Benson, 1995). The node spacing used for the finite difference solution are reported in Table 3.

3. Results and discussion

In order to investigate the effect of helical wrap, a case study of different helix angles varying in the range of $0^\circ \leqslant \beta \leqslant 45^\circ$ is conducted. The web wrap-angle around the reverser is kept constant as $\theta_w = 180^\circ$. Three different *cases* of hole distributions are investigated. In all three cases, the total span of the main hole-regions are kept at 40° in the entry ($|\theta_{F1}–\theta_{F2}|$) and exit ($\theta_{F4}–\theta_{F3}$) directions of the web. In order to investigate the effect of placing the hole-regions in relation to the web's wrap-region, these 40° spans are moved in the circumferential direction, as defined in Table 1. All of the other parameters were kept constant at their values listed in Tables 2 and 3.

3.1. Steady-state solutions

The steady-state conditions predicted by the model for $\beta = 0^\circ$ and 45°, for Case 1, are plotted in Figs. 4 and 5, respectively. The web displacement (w) distribution, measured with respect to the initial wrapped state, is plotted in part (a) of these figures. The air velocity distribution in the fluid domain is given in part (b), where the air pressure (p) contours are also plotted. Finally, the air pressure and contact pressure (p_c) profiles are plotted in 3-D in parts (c) and (d). Note that the same contour legends are used in these figures.

In general, Figs. 4(a) and 5(a) show a large displacement in the central part of the wrap-region, where the web is supported by the air cushion. In the case of $\beta = 0$, the maximum displacement is on the order of 2 mm. But, when the web is wrapped with a helix angle of $\beta = 45^\circ$, the maximum web displacement is found to be approximately 8 mm. In both of these figures, the air cushion support is insufficient to prevent web contact at the entry end exit regions. This is evidenced by the nonzero contact pressure distribution shown in Figs. 4(d) and 5(d). Note that the nonsmooth

Table 1
The extent of the hole-regions for the three cases discussed in this paper

Case	$\theta_{F1}–\theta_{F2}$	$\theta_{F3}–\theta_{F4}$	Hole density, α
1	-90° to -50°	$50–90^\circ$	0.075
2	-100° to -60°	$60–100^\circ$	0.075
3	-110° to -70°	$70–110^\circ$	0.075

See Figs. 1 and 2(a) for the definitions of the angles θ_{Fi}. In addition, holes were placed along the lateral edges spanning $0 \leqslant y \leqslant 5$ cm and $45 \leqslant y \leqslant 50$ cm regions with $\alpha = 0.05$.

Table 2
Parameters common to the presented cases

E (GPa)	4	μ (Pa s)	1.85×10^{-5}
v	0.3	R (m)	0.1
c (mm)	0.05	θ_w (deg.)	180
T_x (N/m)	40	κ	0.9
ρ (kg/m^3)	1	p_0 (kPa)	0.8, 1, 1.2, 1.4

Table 3
Length parameters used for the presented cases

β	0°	5°	10°	15°	20°	30°	40°	45°
L_1 (m)	1	1	1	1	1	1	1	1
$L_x–L_2$ (m)	0.96	0.91	0.87	0.82	0.71	0.58	0.71	0.50
L_x (m)	2.31	2.27	2.23	2.19	2.15	2.07	1.99	1.95
L_y (m)	0.50	0.50	0.50	0.51	0.51	0.51	0.51	0.50
$\Delta x = \Delta y$ (mm)	5.78	5.68	5.58	5.48	5.38	5.18	4.96	4.87
$\Delta x'$ (cm)	0.88	0.90	1.11	1.25	1.39	1.75	2.21	2.48
$\Delta y'$ (cm)	1.24	1.25	1.26	1.26	1.26	1.27	1.27	1.24

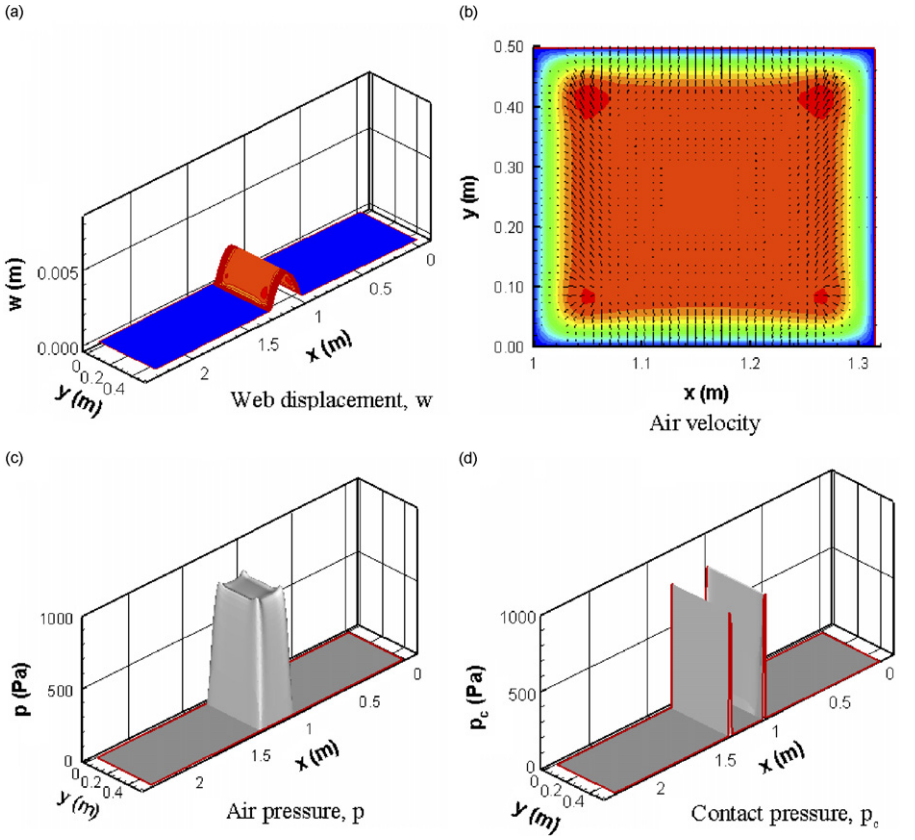

Fig. 4. (a) The web deflection w, (b) airflow vectors, (c) air pressure p and (d) contact pressure p_c at steady state, for Case 1, with $\beta = 0$ and $p_0 = 800\,\text{Pa}$.

contact pressure in these figures is due to numerical discretization. Nevertheless, the web is supported in the central wrap-region by the air cushion. In the case of zero helix angle, Fig. 4(c) shows that, in the central region, the air pressure settles to approximately 800 Pa; the pressure drops to ambient in a narrow transitional region around the outer periphery of the wrap-region. On the other hand, the air pressure for the helix angle of $\beta = 45^\circ$ settles to approximately 450 Pa in the central wrap-region. The pressure drops to ambient in a similar manner around the outer periphery.

3.2. Contact

Fig. 6(a) shows web/turn-bar clearance h, air pressure p and contact pressure p_c along the centerline of the web $(x,0.5L_y)$ for Case 1 and $\beta = 45^\circ$. This figure shows that near the entry and exit regions, the air pressure is insufficient to balance the *belt-wrap pressure* $(T\cos^2\beta/R_w)$ and contact occurs between the web and the turn-bar surface. For this case, the maximum contact pressure is on the order of 400 Pa. In the contact region the clearance h is on the order of the assumed contact height $\sigma_a = 100\,\mu\text{m}$. This allows minimal amount of airflow from the circumferential edges when contact occurs, as observed in Figs. 4(b) and 5(b).

It is concluded that the hole distribution described by Case 1 is inadequate to prevent contacts. Fig. 6(b) shows a comparison of the web/turn-bar clearance h, and air pressure p distributions along the centerline of the web for Cases 1, 2 and 3. Note that contact pressures, which occur for Cases 1 and 2 are omitted from this figure for clarity. Nevertheless, presence of contact can be deduced from the low h values. This figure demonstrates that as the circumferential hole-regions are moved outward to enclose the tangency points ($\theta_w = -90^\circ$ and 90°) of the web, the contact region diminishes, and for Case 3 no contact occurs between the web and the turn-bar.

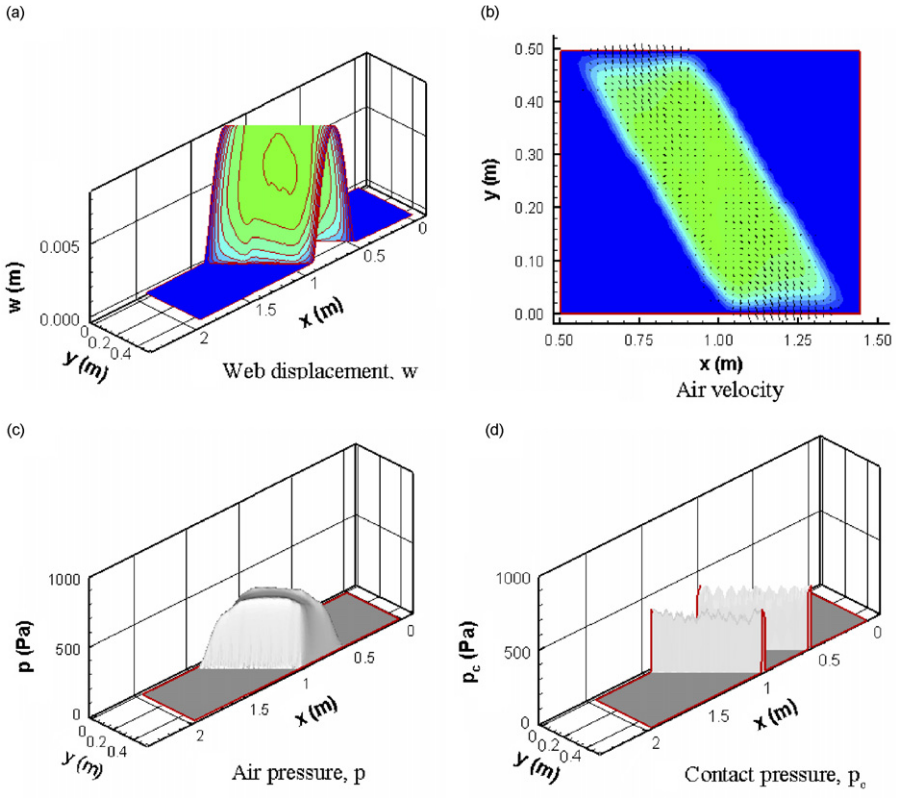

Fig. 5. (a) The web deflection w, (b) airflow vectors, (c) air pressure p and (d) contact pressure p_c at steady state, for Case 1, with $\beta = 45^\circ$ and $p_0 = 800$ Pa.

3.3. *Effect of supply pressure, p_0 and hole distributions*

The supply pressure is one of the easiest design parameters to change. Next, the effects of using different p_0 (800, 1000, 1200, 1400 Pa) values on the equilibrium conditions are investigated, for different designs. Figs. 7 and 8 show web/turn-bar clearance h and air pressure p along the centerline of the web, for different helix-angles $\beta = 0^\circ$, 15°, 30°, and 45° for all three hole-distribution cases considered in Table 1. In particular, Fig. 7 shows equilibrium conditions for supply pressure $p_0 = 800$ Pa, and Fig. 8 for $p_0 = 1200$ Pa. The contact pressure distributions, for the cases where they occur, have been kept out of the pressure plots for clarity. As before, presence of contact can be deduced from the plots of h, where the h value becomes very close to zero.

For the hole-distribution Case 1, Fig. 7(a) shows, that the air cushion provided by the supply pressure of 800 Pa is insufficient to overcome the belt-wrap pressure, and the web contacts the reverser surface near the tangency lines. This figure also shows that, as the helix angle is increased, the web clearance in the central region of the wrap becomes larger, but the air pressure becomes lower. Figs. 7(b) and (c) show the equilibrium conditions for hole-distribution Cases 2 and 3. While a little improvement is seen with respect to preventing contact in Case 2, none of the cases presented in Case 3 contact the turn-bar. Comparison of all three cases in Figs. 7(a)–(c), show that the hole distribution defined by Case 3 provides a more uniform web/turn-bar clearance in the circumferential direction.

The effect of using a supply pressure of 1200 Pa on the same three cases is presented in Fig. 8. Here, we see that Case 1 (Fig. 8(a)) is still inadequate for contact prevention, while Cases 2 and 3, given in Figs. 8(b) and (c), successfully eliminate all contact for all helix angles. It is again observed that Case 3 provides a more uniform h distribution as compared to Case 2.

The results of all the supply pressures $p_0 = 800$–1400 Pa are summarized in Fig. 9. This figure shows the mid-point web/turn-bar clearance $h_{\text{mid}} = h(0.5L_x, 0.5L_y)$ and the minimum clearance h_{min} as a function of the helix angle β and supply pressure p_0. In general, this figure shows that the mid-point clearance increases with increasing supply pressure and increasing helix angle. However, for only Case 3 (Fig. 9(c)) is the minimum clearance entirely larger than zero. In

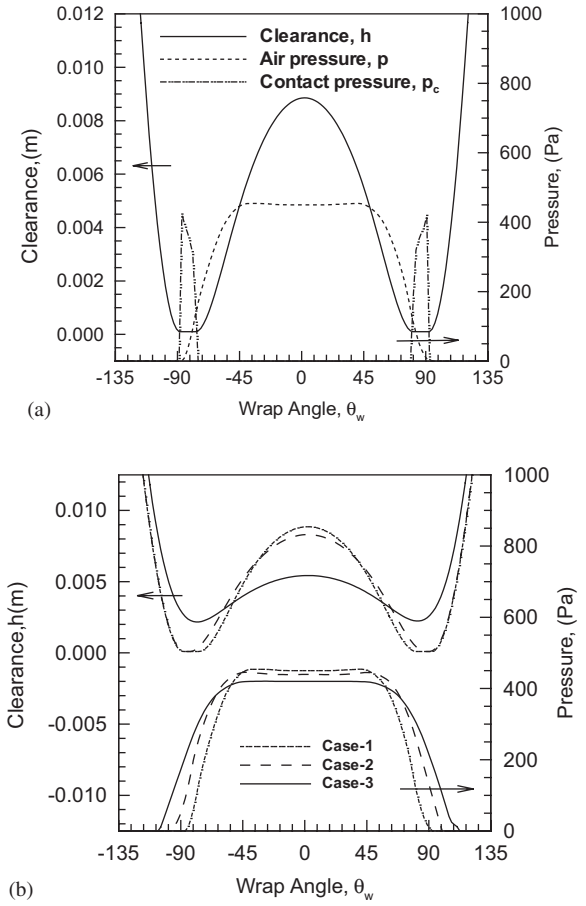

Fig. 6. (a) The web/turn-bar clearance h, air pressure p and contact pressure p_c variation along the centerline (x, $L_y/2$) of the web for Case 1, with $\beta = 45^\circ$ and $p_0 = 800$ Pa. (b) The web/turn-bar clearance and air pressure for Cases 1, 2, and 3 for the same conditions.

Case 2 (Fig. 9(b)), the minimum clearance can be improved by increasing supply pressure; and, in fact, $p_0 = 1200$ and 1400 Pa cases are predicted not to contact. On the other hand, the hole distribution of Case 1 shows no improvement with p_0. It will also be seen in Fig. 9(c) that the h_{mid} and h_{min} values are relatively close to each other. This is due to the fact that the clearance variation in the circumferential direction is fairly uniform, as shown in Figs. 7(c) and 8(c).

3.4. *Effect of helix-angle β on equilibrium*

Figs. 4 and 5 showed that the equilibrium air pressure and web displacements are strongly influenced by the helix angle. At the low value of $\beta = 0$ (Fig. 4), the steady-state pressure reaches 800 Pa, whereas at the high value of $\beta = 45^\circ$ (Fig. 5), it settles to 450 Pa. Conversely, these figures show that the web displacement is lower for low values of β, whereas it is higher for higher β values. In fact, as the helix angle increases from 0° to 45° the web displacement increases while the maximum pressure decreases. This may at first seem counter-intuitive; However, it is actually due to the β dependence of the shell stiffness and the belt-wrap pressure. Eq. (21) shows that the *shell stiffness* and the *belt-wrap pressure* for the helically wrapped web are defined as

$$D_t(\cos^4\beta + \nu\cos^2\beta\sin^2\beta) \quad \text{and} \quad \frac{T\cos^2\beta}{R_w},$$

respectively. Thus, it can easily be seen that the effect of both of these parameters is reduced when $\beta > 0$. As the belt-wrap pressure is reduced at higher β values, the overall equilibrium is established at lower air pressure levels. Similarly, the shell stiffness is also reduced as a result of increasing β, resulting in a more compliant web behavior.

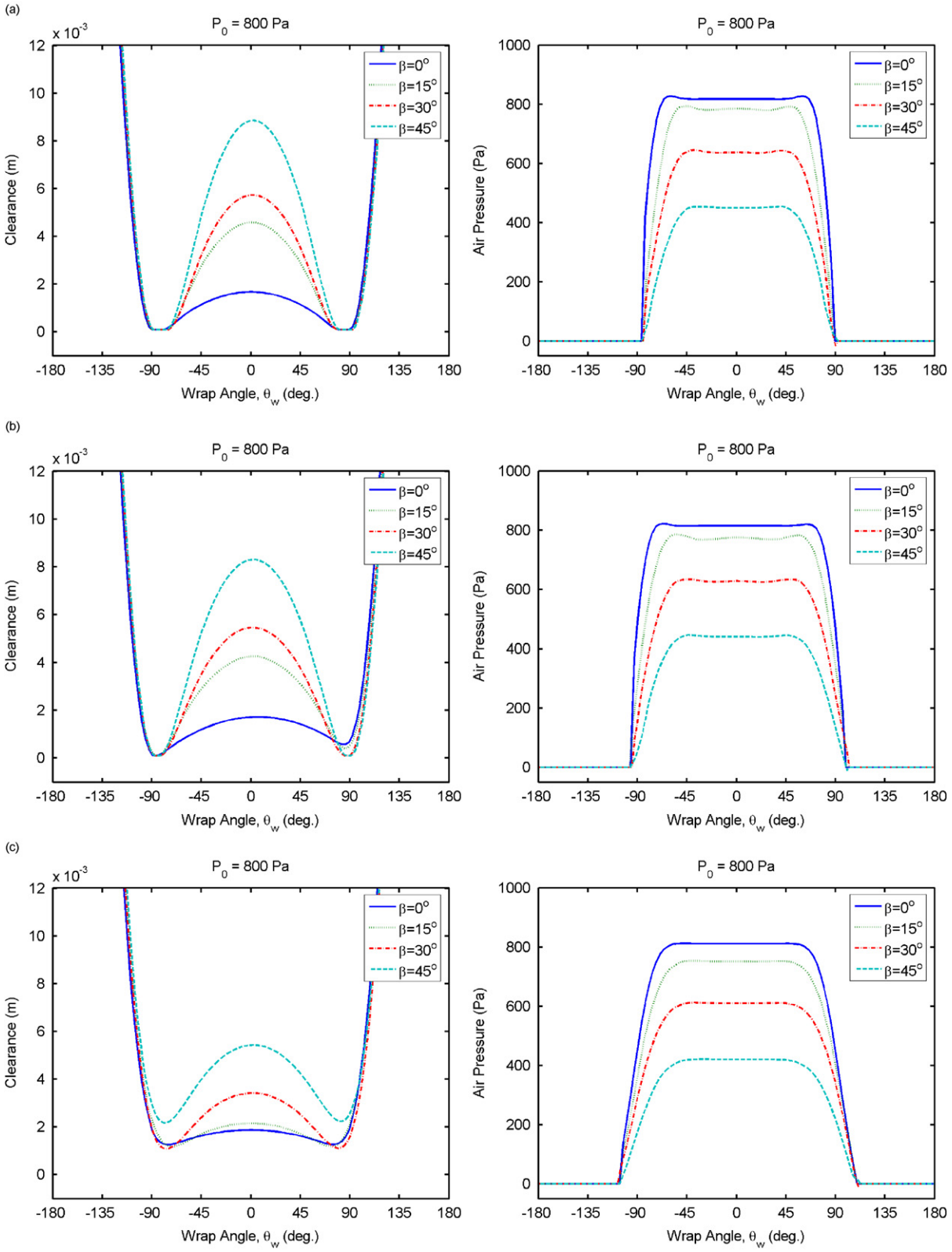

Fig. 7. The web-turn-bar clearance h and air pressure p distributions along the centerline (x, $L_y/2$) for hole distribution (a) Case 1, (b) Case 2 and (c) Case 3. Supply pressure, $p_0 = 800\,\text{Pa}$, and the helix angles (β) are as indicated.

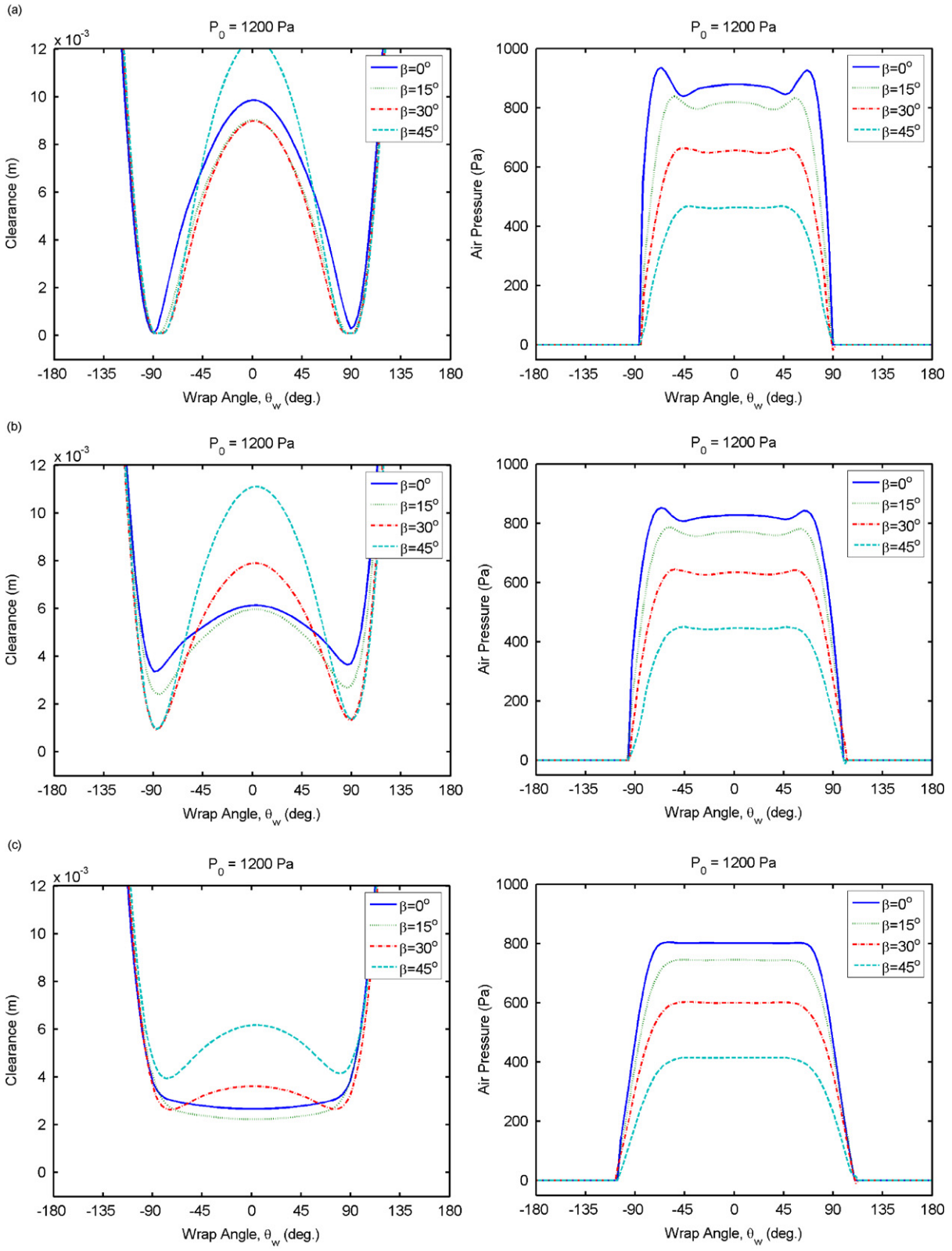

Fig. 8. The web-turn-bar clearance h and air pressure p distributions along the centerline (x, $L_y/2$) for hole distribution (a) Case 1, (b) Case 2 and (c) Case 3. Supply pressure, $p_0 = 1200$ Pa, and the helix angles (β) are as indicated.

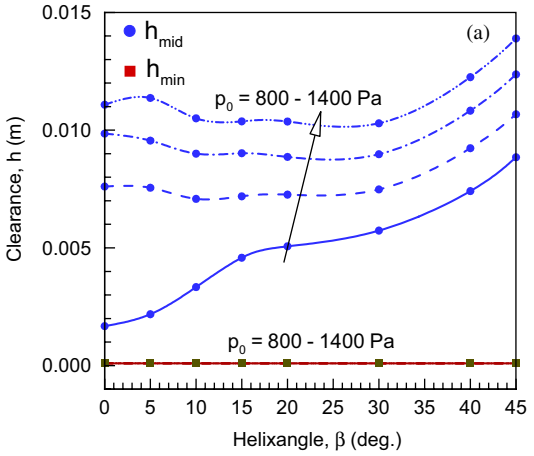

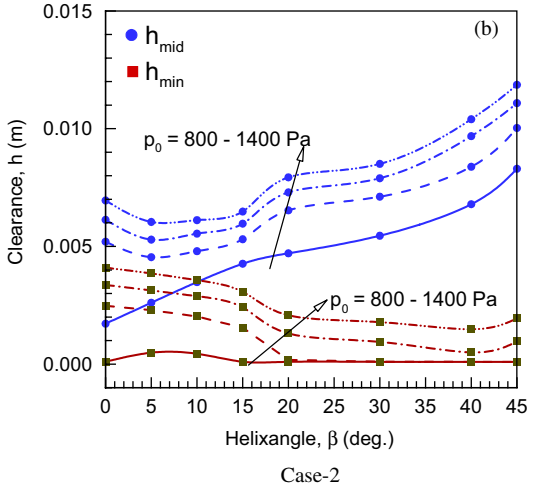

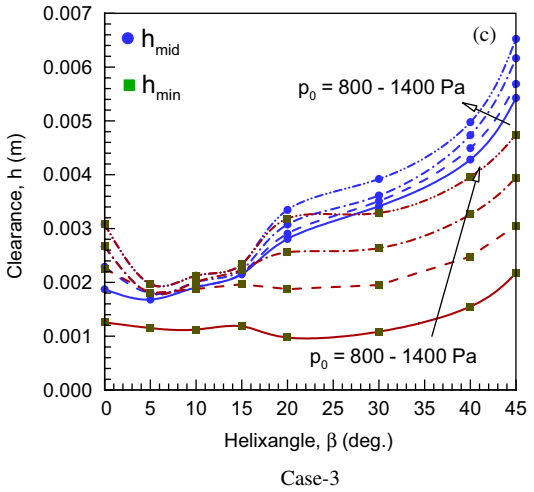

Fig. 9. Variation of mid-point web/turn-bar clearance h_{mid} and minimum web/turn-bar clearance h_{min} for (a) Case 1, (b) Case 2, and (c) Case 3 with different supply pressures p_0 and helix angles, β.

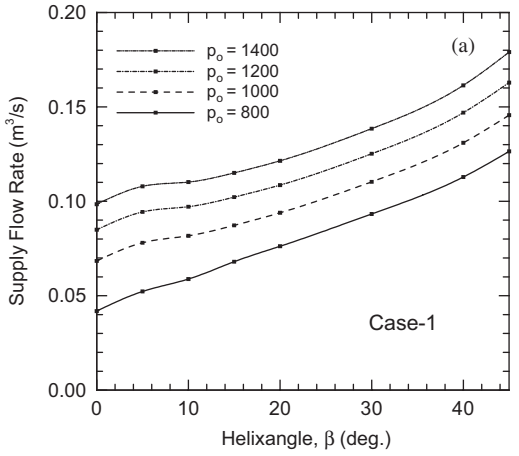

Case 1

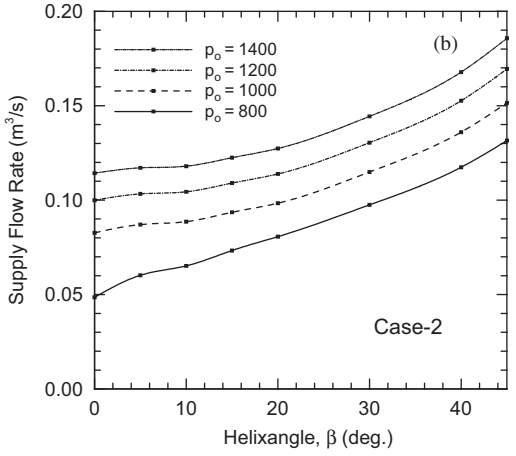

Case 2

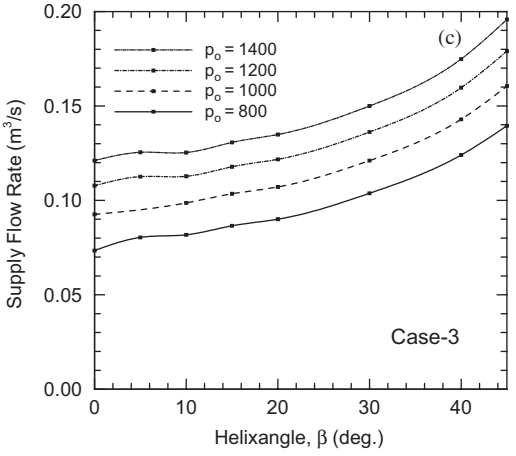

Case 3

Fig. 10. Variation of the supply flow rate Q_{in} for (a) Case 1, (b) Case 2, and (c) Case 3 with different supply pressures p_0 and helix angles, β.

3.5. Flow rate

The supply flow rate into the web/turn-bar interface depends on the local air pressure interface and the discharge coefficient:

$$Q_{\text{in}} = \int_{\Omega_f} U\alpha \, \mathrm{d}\Omega_f.$$

The flow rates for the three cases considered here were evaluated for different p_0 and β values, and they are reported in Fig. 10. The flow rate for all the cases vary in the range of $0.04 \leqslant Q_{\text{in}} \leqslant 0.2\,\text{m}^3/\text{s}$. The flow rate increases with increasing helix angle. This is primarily due to increasing surface area of the circumferential hole-regions at larger helix angles. The flow rate also increases monotonically with increasing supply pressure. The hole-discharge velocity U depends on local air pressure p and supply pressure p_0 as given in Eq. (26). Thus, increasing flow-rate with increasing pressure is an expected result.

4. Summary

A mathematical model for the steady-state deformations of a web wrapped around a turn-bar in a helical fashion is developed. The web is modeled as a thin cylindrical shell. The fluid mechanics is modeled by a modified form of the mass and momentum conservation equations, where the flow variables are averaged in the thickness direction, and where the effect of the mass and momentum influx is considered through a distributed source structure. Contact between the web and the turn-bar surface is considered by a nonlinear asperity compliance function. The governing equations of the helically wrapped shell show that the shell stiffness and the belt-wrap pressure are both reduced as the helix angle is increased. The coupled system is solved numerically. A case study shows the helix angle has a strong influence on the equilibrium configurations; increasing helix angle results in increased web-reverser separation while the air pressure settles to a lower value. This behavior is due to the reduced shell stiffness and belt-wrap pressure for the helically wrapped webs.

It is shown that, in order to prevent web-scratches, it is advantageous to place the hole-regions circumferentially, on the reverser, in such a way that they enclose the tangency points of the web. Conditions that render a fairly uniform web/turn-bar clearance in the circumferential direction are identified.

The airflow rates were found to be on the order of 0.04–$0.2\,\text{m}^3/\text{s}$ for parameters considered in this paper. The flow rates increase with increasing helix angle and supply pressure values. Future work should include transient effects and dynamic stability of the web.

Acknowledgment

The author is grateful for the research grant provided to the Northeastern University by the Eastman Kodak Company in partial support of this work.

References

Ducotey, K.S., Good, J.K., 1999. Predicting traction in web handling. ASME Journal of Tribology 121, 618–624.

Gross, W.A., 1980. Fluid Film Lubrication. Wiley, New York.

Hashimoto, H., Nakagawa, H., 2001. Improvement of web spacing and friction characteristics by two types of stationary guides. ASME Journal of Tribology 123, 509–518.

Lacey, C., Talke, F., 1992. Measurement and simulation of partial contact at the head/tape interface. ASME Journal of Tribology 144, 646–652.

Müftü, S., 1999. Numerical solution of the equations governing the steady state of a thin cylindrical web supported by an air cushion. In Proceedings of the ASME Noise Control and Acoustics Division-1999, NCA-Vol. 26, pp. 425–434.

Müftü, S., Altan, M.C., 2000. Mechanics of a porous web moving over a rigid guide. ASME Journal of Tribology 122, 418–426.

Müftü, S., Benson, R.C., 1995. Modelling the transport of paper webs including the paper permeability effects. In Proceedings of the Information Storage and Processing Systems Symposium, ASME International Congress and Exposition, San Francisco, CA, pp. 247–258.

Müftü, S., Cole, K.A., 1999. The fluid/structure interaction of a thin flexible cylindrical web supported by an air cushion. Journal of Fluids and Structures 13, 681–708.

Müftü, S., Lewis, T.S., Cole, K.A., 1997. A numerical solution of the Euler's equations with nonlinear source terms in modeling the fluid dynamics of an air reverser. In Proceedings of the Information Storage and Processing Systems Symposium, International Congress and Exposition, Dallas, TX, ISPS-3, pp. 39–48.

Müftü, S., Lewis, T.S., Cole, K.A., Benson, R.C., 1998. A two dimensional model of the fluid dynamics of an air reverser. ASME Journal of Applied Mechanics 65, 171–177.

Rice, B., Cole, K.A., Müftü, S., 2002. A model for determining the asperity engagement height in relation to web traction over non-vented rollers. ASME Journal of Tribology 124 (3), 584–594.

Rongen, P.M.J., 1994. Finite element analysis of the tape scanner interface in helical scan recording. Ph.D. Dissertation, Technische Univesiteit Eindhoven, The Netherlands

Schilchting, H., 1987. Boundary-Layer Theory. McGraw-Hill, New York.

Timoshenko, S.P., Woinkowsky-Krieger, S., 1987. Theory of Plates and Shells. McGraw-Hill, New York.

Wu, Y., Talke, F., 1996. The effect of surface roughness on the head-tape interface. ASME Journal of Tribology 118, 376–381.